RSC Advances

PAPER

View Article Online
View Journal | View Issue

Cite this: *RSC Adv.*, 2014, **4**, 61363

New ternary bipyridine–terpyridine copper(II) complexes as self-activating chemical nucleases†

Sofia Gama,*[a] Inês Rodrigues,[a] Fernanda Marques,[a] Elisa Palma,[b] Isabel Correia,[b] M. Fernanda N. N. Carvalho,[b] João Costa Pessoa,[b] Andreia Cruz,[c] Sónia Mendo,[c] Isabel C. Santos,[a] Filipa Mendes,[a] Isabel Santos[a] and António Paulo[a]

Received 9th October 2014
Accepted 4th November 2014

DOI: 10.1039/c4ra12085j

www.rsc.org/advances

Seeking self-activating chemical nucleases with potential applications as therapeutic agents, new ternary terpyridine–bipyridine–Cu(II) complexes carrying pendant cyclic amines were developed. After detailed characterization, the nuclease activity of the synthesized compounds was evaluated by using circular plasmid DNA as substrate and analyzing the products by agarose-gel electrophoresis. The new complexes present an impressive plasmid DNA cleaving ability, which triggers double-strand DNA breaks in the absence of any exogenous agents, *via* an oxidative mechanism. The binding affinity towards duplex DNA was determined using UV-Vis and fluorescence spectroscopic titrations. These studies showed that the tested complexes bind moderately (in the order of 10^4 M^{-1}) to duplex DNA. The copper complexes displayed high cytotoxicity against ovarian carcinoma A2780 cells (4-fold cisplatin activity), surpassing the resistance on the cisplatin-resistant cell line (A2780cisR) with lower resistance factors. Cellular uptake studies showed that the ternary complexes were able to enter the cell with a significant localization in the cytoskeleton.

1 Introduction

There has been considerable interest in recent years in the development of DNA cleaving reagents due to their potential application in biotechnology and medicine.[1] DNA damage by exogenous molecules, mostly *via* oxidative or hydrolytic mechanisms, is an important process in cellular systems, because the resulting lesions may have a significant influence on the physiological/biological function of DNA. Importantly, in the absence of an efficient repair mechanism, DNA damage may lead to mutagenesis, carcinogenesis, cell death or aging.[2]

DNA cleavage induced by metal complexes recently attracted much attention, since the modes of action of these reagents resemble the ones employed by naturally occurring nucleases.[2] Nucleases are ubiquitous enzymes indispensable for cellular and viral development, acting at the DNA- (DNAses) and the RNA-level (RNAses). They are known to be involved on the control of several biological processes, namely protective mechanisms against "foreign" (invading) DNA, degradation of host cell DNA after viral infection, DNA repair, DNA recombination, DNA synthesis, DNA packaging in chromosomes and viral compartments and maturation of RNAs or RNA splicing.

Unsurprisingly, one of the challenges that has engaged many chemists over the last years is the development of the so-called "artificial nucleases". These are, or should be, synthetic systems able to reproduce the activity of hydrolytic enzymes that cleave phosphate esters.[3] Chemists have been searching for low-molecular weight synthetic mimics of such enzymes, not only to help to improve the fundamental understanding of mechanistic aspects of enzyme action, but also to develop new biotechnological tools (artificial restriction enzymes and footprinting agents) and nucleic acid-targeting therapeutics.[2] The last few years have seen substantial progress as new approaches have been described and the first applications of artificial hydrolytic agents to DNA manipulation have been reported.[3]

The knowledge that the active site of most nucleases contain divalent cations, such as Mg^{2+}, Ca^{2+}, Mn^{2+} or Zn^{2+}, prompted a massive amount of research aimed at discovering new metal complexes capable of mimicking the hydrolytic activities of metallo-nuclease enzymes. The diverse structural features and versatility shown by transition metal-based compounds, such as multiple/variable oxidation states and redox properties make them good candidates to be exploited to discover novel artificial nucleases. Among the first row transition elements, copper has elicited a special interest since the discovery of first chemical nuclease by Sigman *et al.*[4] Together with the possibility of damaging DNA by hydrolytic and/or oxidative mechanisms,

[a]*Centro de Ciências e Tecnologias Nucleares (C²TN), Instituto Superior Técnico, Universidade de Lisboa, Campus Tecnológico e Nuclear, Estrada Nacional 10 (km 139,7), 2695-066, Bobadela LRS, Portugal. E-mail: scgama@ctn.ist.utl.pt*

[b]*Centro de Química Estrutural, Instituto Superior Técnico, Universidade de Lisboa, Avenida Rovisco Pais 1, 1049-001 Lisboa, Portugal*

[c]*Departamento de Biologia & CESAM, Universidade de Aveiro, Campus de Santiago, 3810-193 Aveiro, Portugal*

† CCDC 1017524–1017525. For crystallographic data in CIF or other electronic format see DOI: 10.1039/c4ra12085j

copper complexes may additionally induce efficient cleavage of DNA due to their high nucleobase affinity and the relatively strong Lewis acidity of Cu(II) ions.[1,2]

For most copper complexes exhibiting strong DNA cleavage activity, the activity is mediated by reactive oxygen species (ROS) produced *via* the oxidation of Cu(II) to Cu(III) by the addition of external oxidizing agents (*e.g.* dihydrogen peroxide, molecular oxygen) or the reduction of Cu(II) to Cu(I) by a reductive reagent (*e.g.* ascorbic acid, 3-mercaptopropionic acid).[5,6] Transient-metal-bound species formulated as $[CuOH]^{2+}$, $[CuOOH]^{+}$, and $[CuO]^{+}$ have also been reported as responsible for DNA strand scission.[5] Additionally, copper complexes with appropriate ligand(s), can cleave DNA without any external agent, but often photo-induction is needed to initiate the cleavage process.[6] For the above described reasons, the *in vivo* application of these reagents is limited since the addition of an oxidizing or reducing agent or the use of photoactivation are not readily feasible and attractive. Therefore, it would be of great interest to find self-activated systems not requiring any type of activation to generate reactive species for DNA cleavage activity.

Only a few reports on nuclease activity *via* self-activation have been published[5–17] but recently copper complexes, possessing inherently diverse structural and redox properties, emerged as attractive self-activating agents for DNA cleavage.[1,5,6,12–16,18]

In the past few years, several copper complexes have been proposed as potential anticancer metallodrugs, demonstrating remarkable anticancer activity and showing toxicity generally lower than platinum compounds.[19] In particular, mixed ligand copper(II) complexes were found to exhibit prominent anticancer activity by inducing apoptosis, strongly binding and cleaving DNA.[20] Inspired by these findings, we developed a new family of ternary bipyridine–terpyridine–copper(II) complexes [Bpy–Tpy–Cu(II)] containing pendant cyclic amine groups. The cyclic amines introduced at the pyridine ligands were expected to enhance the DNA binding affinity of the complexes by electrostatic interactions between the protonated amines and the phosphodiester backbone of the nucleic acid. Herein, we report on new bipyridine derivatives functionalized with different cyclic amine groups (pyrrolidine, piperazine and morpholine) and on their ternary Bpy–Tpy–Cu(II) complexes. The action of these ternary complexes as self-activating DNA nucleases was evaluated and, additionally, their biological behavior in human cancer cell lines was correlated to their biophysical properties and cellular uptake.

2 Results and discussion

2.1. Synthesis, characterization, spectral and redox properties

The bipyridine compounds were synthesized by reaction of chloro alkyl derivatives of the corresponding cyclic amine with the 2,2′-bipyridine-4,4′-diol precursor, in a 2 : 1 ratio, as depicted in Scheme 1. The diol precursor was obtained by cleavage *via* hydrobromic acid of 4,4′-dimethoxy-2,2′-bipyridine, as described in the literature.[21]

The ternary Bpy–Tpy–Cu(II) complexes ($\mathbf{C^2}$–$\mathbf{C^4}$) containing pendant cyclic amines could be obtained in one step by reacting stoichiometric amounts of the desired bipyridine derivative and terpyridine with copper(II) triflate, in acetonitrile at room temperature (Scheme 2). This approach was reported previously for the synthesis of the parental complex $\mathbf{C^1}$, which contains a pentacoordinated metal atom bound to one tridentate terpyridine and one bidentate bipyridine ligand.[22] Compound $\mathbf{C^1}$ was also synthesized in this work aiming to compare its nuclease activity with that exhibited by the congeners containing pendant cyclic amines. The formation of complexes $\mathbf{C^1}$–$\mathbf{C^4}$ was almost immediate as indicated by the sudden appearance of a blue color upon addition of ligands. The complexes precipitated from each reaction mixture as microcrystalline blue solids, after counterion exchange with hexafluorophosphate and addition of diethyl ether. Further purification was achieved by recrystallization, through diffusion of diethyl ether into acetonitrile solutions of the complexes.

The formulation of compounds $\mathbf{C^2}$–$\mathbf{C^4}$ as ternary bipyridine–terpyridine–copper(II) complexes was established on the basis of their characterization by elemental analysis, MALDI-TOF mass spectrometry, EPR and single crystal X-ray diffraction analysis (for $\mathbf{C^3}$ and $\mathbf{C^4}$). In particular, the MALDI-TOF spectra of all the complexes showed peaks with m/z values corresponding to the respective $[M^+]$ molecular ion and displaying isotopic distribution patterns consistent with the presence of copper.

X-ray quality crystals of $\mathbf{C^3}$ and $\mathbf{C^4}$ were obtained by recrystallization from saturated solutions of the compounds in acetonitrile. Complex $\mathbf{C^3}$ crystallized in the triclinic system, space group $P\bar{1}$, and $\mathbf{C^4}$ crystallized in the monoclinic system, space group $P2_1/n$. The crystal data and final refinement details for complexes $\mathbf{C^3}$ and $\mathbf{C^4}$ are given in Table 1. A selection of bond lengths and angles are given in Table 2. The respective ORTEP diagrams are presented in Fig. 1.

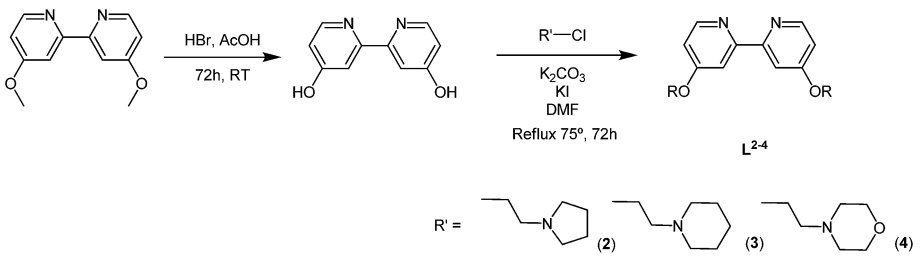

Scheme 1

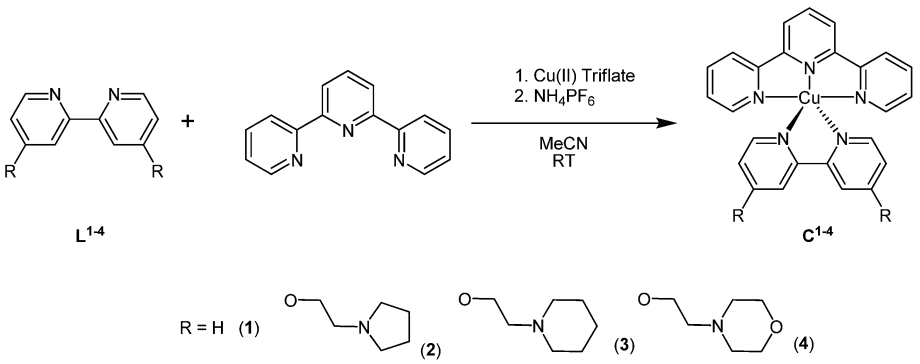

Scheme 2

The X-ray structural analysis of $\mathbf{C^3}$ and $\mathbf{C^4}$ confirmed that the central Cu(II) metal ion in each of these complexes is penta-coordinated by tridentate terpyridine (tpy) and bidentate 2,2′-bipyridine (bpy) ligands. The coordination polyhedron is best described as a distorted square-pyramidal with an N atom from the bipyridine ligand in the apical position. The angle between the basal plane defined by N1 N2 N3 N5 atoms and the Cu1–N4 apical bond is 72.7(2)° in both compounds; the Cu1–N4 apical bond (2.160(4) Å and 2.179(5) Å) is longer than the Cu1–N5 equatorial bond distance (1.976(5) Å and 1.986(4) Å) for the coordinated bipyridine nitrogen atoms in the complexes $\mathbf{C^3}$ and $\mathbf{C^4}$, respectively. In the complex $\mathbf{C^4}$, the atoms of both morpholinyl containing arms (C26C27–C26aC27a and O2C32C33–O2aC32aC33a) are disordered over two sites (0.57–0.43 and 0.45–0.55) respectively.

In the crystal packing of $\mathbf{C^3}$ and $\mathbf{C^4}$, hexafluorophosphate counter-ions are involved as acceptors in several intermolecular C–H···F hydrogen-bonding interactions with both the bipyridyl and terpyridyl ligands, resulting in a three-dimensional supramolecular structure (Fig. 2). The same extensive network of hydrogen bonds was found by Ulrich S. Schubert in the solid state structure of the parental complex $\mathbf{C^1}$.[22] Dai-Zhi Kuang *et al.*[23] have also reported on related Cu(II) complexes containing a tridentate 4′-ferrocenyl-2,2′:6′,2″-terpyridine and a bidentate 2,2′-bipyridine ligand, which crystallizes with formation of similar three-dimensional supramolecular structures.

Table 1 Crystallographic data and structure refinement parameters for compounds $\mathbf{C^3}$ and $\mathbf{C^4}$

	$\mathbf{C^3}$	$\mathbf{C^4}$
Crystal size (mm)	0.60 × 0.30 × 0.04	0.18 × 0.10 × 0.03
Crystal colour and shape	Green, plate	Blue, plate
Temperature (K)	150(2)	150(2)
Empirical formula	$C_{41}H_{48}N_8O_2F_{24}P_4Cu$	$C_{37}H_{40}N_7O_4F_{12}P_2Cu$
Molecular mass	1328.29	1000.24
Crystal system	Triclinic	Monoclinic
Space group	$P\bar{1}$	$P2_1/n$
a (Å)	8.2891(7)	20.9700(7)
b (Å)	17.7944(8)	8.7014(4)
c (Å)	19.6703(10)	28.5460(10)
α (°)	78.996(2)	90
β (°)	85.893(2)	91.070(2)
γ (°)	89.038(2)	90
V (Å^3)	2840.7(3)	5207.8(3)
Z, D_{calcd} (Mg m^{-3})	2, 1.553	4, 1.276
μ (mm^{-1})	0.618	0.563
F(000)	1342	2040
Theta range (°)	3.40 to 25.03	2.92 to 25.03
Index range (h, k, l)	−5/9, −21/21, −23/23	−24/24, −10/10, −33/33
Refl. collected/unique	17 125/9746 [R_{int} = 0.04]	32 880/9061 [R_{int} = 0.0731]
T max./min.	0.9757/0.7080	0.9458/0.8673
Data/restr/param	9746/0/722	9061/19/541
G.O.F. on F^2	1.010	0.958
R [$I > 2\sigma(I)$]	$R1$ = 0.0827, w$R2$ = 0.2160	$R1$ = 0.0996, w$R2$ = 0.2543
$\Delta\rho$ max/min [eA^{-3}]	1.29/−0.842	1.074/−0.582

The EPR spectra of complexes $\mathbf{C^1}$–$\mathbf{C^4}$ measured from DMSO solutions frozen at 77 K (Fig. 3) show axial symmetry with a more intense absorption at higher field ($g_\perp$) and a less intense one at lower field ($g_\parallel$). The spin Hamiltonian parameters $g_\parallel$ and $A_\parallel$ depend, among other factors, on the nature of the donor atoms, and can be used to confirm the binding mode around the metal ion. The simulation of the experimental spectra resulted in good spectral fit and reliable spin Hamiltonian parameters that are in agreement with those published for other terpyridine or bipyridine Cu(II) complexes.[24,25] The values obtained for the $g_\parallel$ and $A_\parallel$ (Table 3) are in agreement with the expected for coordination of copper to nitrogen atoms only.[26,27] No superhyperfine coupling with the nitrogen donors could be observed, due to the low bandwidth resolution, which is common in solvents with high viscosity such as DMSO.

As the nuclease effect induced by most of the known metallonucleases often proceeds *via* redox cycles between different oxidation states of the metal ions, the redox behavior of the copper complexes $\mathbf{C^1}$–$\mathbf{C^4}$ was studied by cyclic voltammetry. Representative cyclic voltammograms for $\mathbf{C^2}$ and $\mathbf{C^3}$ are displayed in Fig. 4. Three distinct regions are observed for all complexes, except $\mathbf{C^1}$. The first region (I) displays cathodic waves at relatively accessible reduction potentials (−0.20 to −0.23 V) with quasi-reversible character ($^{I}E^{red}_{1/2}$), which are preceded by shoulder waves at slightly higher potential; the second region (II) shows irreversible waves ($^{II}E^{red}_{p}$) in the range

Table 2 Selected bond lengths (Å) and angles (°) for complex C^3 and C^4

Bond lengths (Å)				Bond angles (°)			
C^3		C^4		C^3		C^4	
Cu1–N1	2.047(5)	Cu1–N1	2.064(6)	N1–Cu1–N2	80.44(19)	N1–Cu1–N2	80.8(2)
Cu1–N2	1.915(4)	Cu1–N2	1.908(5)	N1–Cu1–N3	158.41(19)	N1–Cu1–N3	159.3(2)
Cu1–N3	2.065(5)	Cu1–N3	2.040(5)	N1–Cu1–N4	106.68(18)	N1–Cu1–N4	95.51(19)
Cu1–N4	2.160(4)	Cu1–N4	2.179(5)	N1–Cu1–N5	98.7(2)	N1–Cu1–N5	100.1(2)
Cu1–N5	1.976(5)	Cu1–N5	1.986(4)	N2–Cu1–N3	80.4(2)	N2–Cu1–N3	79.3(2)
				N2–Cu1–N4	110.06(18)	N2–Cu1–N4	115.2(2)
				N2–Cu1–N5	170.13(19)	N2–Cu1–N5	166.5(2)
				N3–Cu1–N4	89.15(19)	N3–Cu1–N4	98.2(2)
				N3–Cu1–N5	98.5(2)	N3–Cu1–N5	98.5(2)
				N4–Cu1–N5	79.66(18)	N4–Cu1–N5	78.30(19)

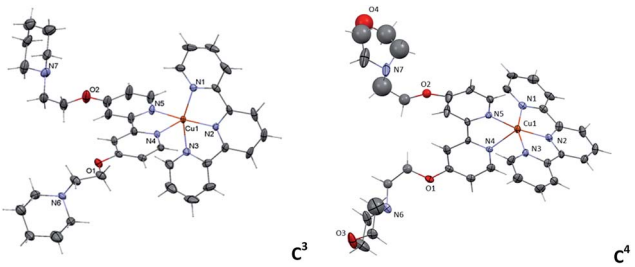

Fig. 1 ORTEP diagram of C^3 and C^4. Ellipsoids were drawn at the 40% probability level.

−1.09 to −1.16 V, which are associated with strong adsorption waves on the reverse scan (except for C^4); finally, a third region (III, not observed for C^1) at potentials (−2.22 and −2.30 V) close to the limit of the potential window (Table 4) is registered. Region III is omitted for clarity in the cyclic voltammograms of C^2 and C^3 presented on Fig. 4. These lowest potential reduction waves can be attributed to reduction of the ligands ($^{III}E_p^{red}$),

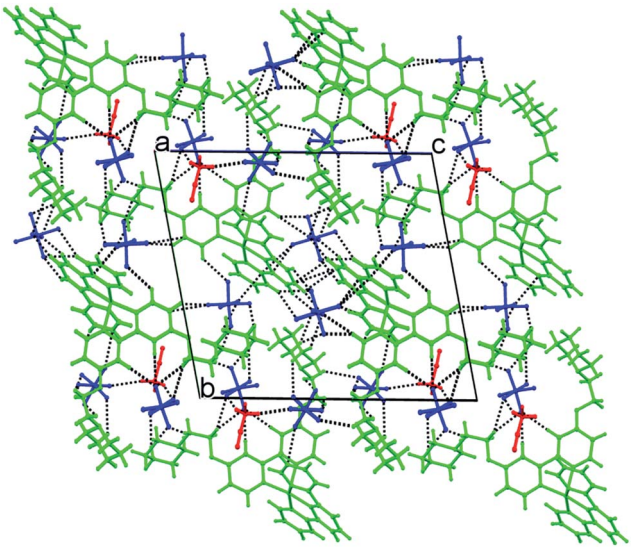

Fig. 2 The crystal structure of C^4. View along the stacking axis *a* emphasizing the short contacts.

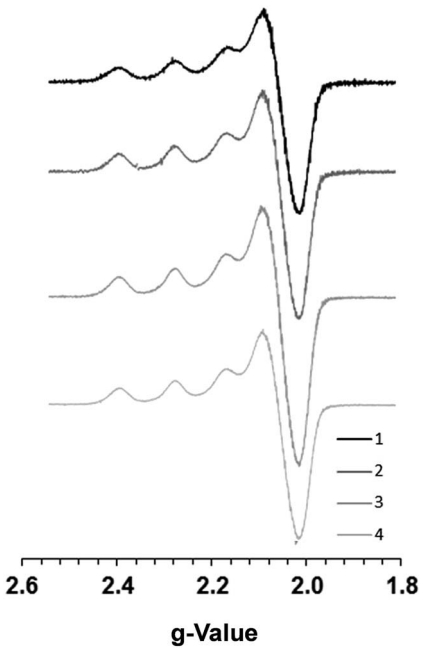

Fig. 3 EPR X-band spectra recorded at 77 K for 5 mM solutions of C^1–C^4 in DMSO.

based on the study of the redox properties of the free ligands that has been performed under identical experimental conditions (Table 4).

Overall, the electrochemical data obtained for complexes C^1–C^4 are consistent with Cu(II) → Cu(I) reductions (region I) followed by Cu(I) → Cu(0) reduction (region II) $^{II}E_p^{red}$. The measured Cu(II)/Cu(I) reduction potentials $^{I}E_{1/2}^{red}$ compare well with those previously reported for related complexes.[30,31] Upon Cu(I) → Cu(0) reduction, the observed adsorption wave gives evidence for decomposition of the complexes with formation of copper metal (Scheme 3).

In summary, the cyclic voltammetry studies of C^1–C^4 have shown that these Cu(II) complexes have very similar redox potentials, despite displaying slight differences in their electrochemical behavior due probably to the irreversible nature observed for some processes. These results can be explained by

Table 3 Spin Hamiltonian parameters for the Cu(II) complexes obtained by simulation of the experimental spectra[28]

EPR parameters				
	$g_{\parallel}$	$g_{\perp}$	$A_{\parallel} \times 10^4$ [cm^{-1}]	$A_{\perp} \times 10^4$ [cm^{-1}]
C^1	2.255	2.066	156.5	11.9
C^2	2.255	2.063	155.4	12.1
C^3	2.255	2.063	156.0	11.6
C^4	2.255	2.062	156.4	11.9

the structural similarity of the studied complexes, that maintain the same coordination environment in solution, as confirmed by the EPR studies discussed above.

2.2. DNA interaction

It has been considered that the interaction of Cu(II) complexes with DNA could play a vital role in their potential cytotoxicity activity. The binding to DNA double helical structures is one of the ways by which anticancer drugs exert its effect. It can be divided in two main categories: covalent and non-covalent, such as electrostatic interaction, intercalation between base pairs and minor and major DNA groove binding interaction. Drugs like cisplatin interact with DNA forming covalent adducts in an irreversible way causing inhibition of DNA processes and subsequent cell death. Although, when concerning drug metabolism and toxicity, reversible non-covalent interactions are typically preferred for anticancer drugs.[32]

To evaluate such interactions several experimental techniques were applied, based on the fact that interactions between DNA and drugs/inorganic compounds can cause chemical and conformational modifications and, thus, variations of the electrochemical properties of nucleobases.[32]

2.2.1. DNA binding. First, UV-Vis and fluorimetric spectroscopic titrations were performed to evaluate the binding affinity and gain some insight on the binding mode of complexes **C^1–C^4** to DNA.

The electronic absorption spectra of complexes **C^1–C^4** (Fig. 5a), measured in PBS buffer (10 mM, pH 7.2) present three strong absorption bands with maxima at 268, 277 and 285 nm, which can be attributed to intraligand transitions. A shoulder at 312 nm and two weaker absorption bands at 326 and 339 nm are also registered, corresponding to the metal-perturbed intraligand π–π* transition.

Table 4 Cyclic voltammetry data[a] obtained for the ligands and Cu(II) complexes

	$^{I}E_p^{red}$	$^{II}E_p^{red}$	$^{III}E_p^{red}$	E_p^{ox}
Terpyridine	—	—	−2.21[b]	No
Bipyridine	—	—	No	No
L^2	—	—	−2.33	0.98
L^3	—	—	−2.32	1.10
L^4	—	—	<−2.5	1.24
C^1	−0.23[c]	−1.09[d]	No	—
C^2	−0.19[e]	−1.18	−2.26	—
C^3	−0.26[e]	−1.22	−2.30	—
C^4	−0.20[f]	−1.16	−2.22	—
$[Cu(bpy)_2]^{2+}$	−0.169[g]	—	—	—

[a] $[NBu_4][BF_4]/CH_3CN$ (0.1 M) as electrolyte. Potentials (±10 mV) quoted *versus* SCE, using $[Fe(\eta^5\text{-}C_5H_5)_2]^{0/+}$ ($E_{1/2}^{ox}$ = 0.382 V)[29] as internal reference. [b] Quasi-reversible wave $E_{1/2}^{red}$ = −2.16 V. [c] Shoulder at $^{I}E_p^{red}$ = −0.011 V. [d] A new wave was formed at E_p^{red} = −0.58 V during the electrochemical study of this complex. [e] Shoulder at $^{I}E_p^{red}$ = −0.12 V. [f] Shoulder at $^{I}E_p^{red}$ = −0.17 V. [g] Ref. 30.

$$[Cu(Tpy)L^{1\text{-}4}]^{4+} \xrightarrow[\text{(wave I)}]{+\,e^-} [Cu(Tpy)L^{1\text{-}4}]^{3+} \xrightarrow[\text{(wave II)}]{+\,e^-} [Cu(Tpy)L^{1\text{-}4}]^{2+} \longrightarrow Cu^0$$

Scheme 3

A simple way to determine whether interactions between DNA and the metal complex are present is to look for changes in the UV-Vis spectrum of the complex upon addition of DNA. As exemplified for **C^3** in Fig. 5b, upon incremental additions of calf thymus DNA (CT-DNA) to the complex solutions, small perturbations in the ligand-centered bands, and a smaller effect in the metal-perturbed intraligand bands are observed. Furthermore, there is no change in the position of the absorption bands (no red shift). This behavior was observed for all the complexes.

The UV-Vis titration experiments have shown that there is no strong intercalative interaction between the complexes and CT-DNA, which is usually characterized by an accentuated red shift and hypochromism. In the case of a strong electrostatic attraction between the compound and DNA, an hyperchromic

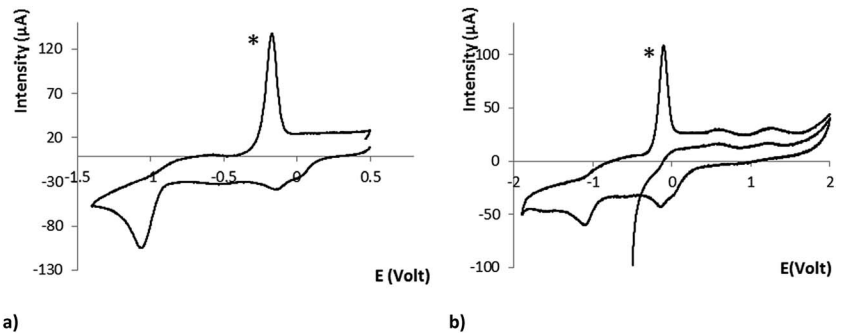

Fig. 4 Representative cyclic voltammograms of (a) **C^2** and (b) **C^3** obtained in CH_3CN. (*) adsorption wave.

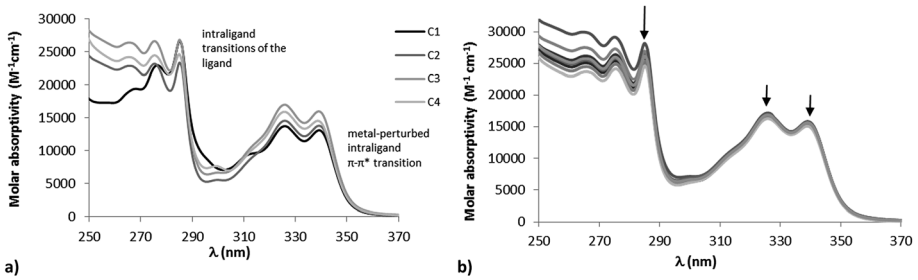

Fig. 5 UV-Vis absorption spectra of (a) Cu(II) complexes (C^1–C^4) and (b) spectrophotometric titration of CT-DNA with complex C^3 (50 μM), in PBS buffer (10 mM, pH 7.2), at room temperature. The arrows indicate the changes of the bands upon addition of CT-DNA ([DNA]/[C^3] = 0–3.2).

effect should be observed, reflecting the alterations in DNA conformation and structure after the complex-DNA interaction has occurred,[33] which is also not the case. The observed small change in the intensity of the intraligand spectral bands may be indicative of a weak interaction, usually characterized by hypochromic or hyperchromic effects without significant wavelength shifts in the spectral profiles.[34]

To quantify and compare the CT-DNA binding affinity of complexes C^1–C^4, their intrinsic binding constants K_b were determined by monitoring the changes in the absorbance of the intraligand bands with increasing concentration of CT-DNA, using a simple Scatchard model (see Experimental section). The calculated binding constant values ($3.7–6.4 \times 10^4$ M^{-1}) are comparable to those reported for other polypyridyl–copper(II) complexes, such as copper(II)–tolyl-terpyridine ($K = 0.84 \times 10^4$ M^{-1}), copper(II)–tolyl-terpyridine-dimethylphenanthroline ($K = 2.3–3.3 \times 10^5$ M^{-1}),[35,36] and copper(II)–terpyridine complexes functionalized with piperidine substituents ($K = 1.35–6.71 \times 10^4$ M^{-1}).[37]

To obtain additional information on the mode of interaction of the complexes with DNA and their physical "localization" relative to the double helix, fluorescence spectroscopy studies were performed, taking advantage of the high sensitivity, large linear concentration range and selectivity of molecular fluorescence.[32] As an example, Fig. 6 shows the effect of the concentration of DNA on the fluorescence emission spectra measured for solutions of complex C^2 (5 μM). Upon addition of increasing amounts of CT-DNA, a decrease of the emission band is clearly observed, as a result of the chromophore (Cu(II) complex) quenching due to the interaction with CT-DNA. This effect was observed with all complexes.

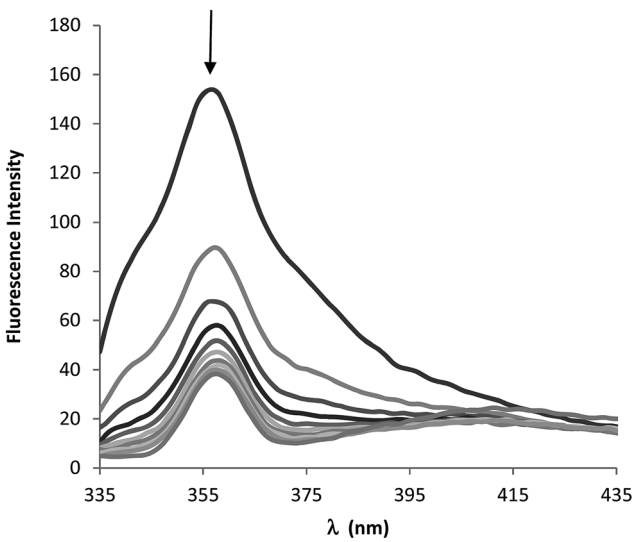

Fig. 6 Fluorescence emission titration of complex C^2 (5 μM) in PBS buffer (pH = 7.4) with CT-DNA. The arrow indicate changes upon addition of increasing amounts of CT-DNA ([DNA]/[C^2] = 0–11).

In the case of intercalating drugs, the molecules are inserted into the base stack of the helix, and the rotation of the free molecules favors the radiationless deactivation of the excited states. Also if the drugs are bound to DNA, the deactivation through fluorescence emission is favored, and a significant increase in the fluorescence emission is normally observed.[38] Nevertheless it is possible to observe a decrease in the fluorescence intensity in the presence of DNA when groove binding, electrostatic, hydrogen bonding or hydrophobic interactions are involved and the molecules are close to the sugar–phosphate backbone. Considering the three widely accepted non-covalent interaction modes between metal complexes and DNA (electrostatic interaction/"outside" binding, groove binding and intercalation binding[39]) the UV-Vis and fluorimetric results indicate that intercalation is not the main process involved in the interaction of C^1–C^4 with CT-DNA.

This conclusion is further supported by DNA melting studies (T_m, the temperature at which the double helix denatures into single strand DNA) made in the absence and presence of the complexes. In the absence of complexes, $T_m = 82.8 \pm 0.5$ °C for CT-DNA. The addition of complexes C^1–C^4 to DNA under identical experimental conditions resulted in a ΔT_m of -0.3 ± 0.5 °C, which is within the experimental error. The intercalation of small molecules into the DNA double helix is known to increase the DNA melting temperature,[40] while the interactions realized *via* non-traditional intercalation, groove binding or electrostatic forces are known to have slight effects on T_m.[41] Therefore, the quite low and small negative ΔT_m values obtained indicate that there is no extra stabilization of the double-stranded nucleic acids by C^1–C^4, giving further support to the conclusion that these complexes and CT-DNA do not interact *via* intercalation.

These observations can be rationalized taking into consideration the structures of C^2–C^4. In each of these complexes, the bipyridine co-ligand carries two protonable aliphatic amines.

According to Pearson's hard/soft acid/base theory, these positively-charged aliphatic amino groups are hard acid, and are most likely capable of binding to the negatively-charged phosphate groups, rather than to the DNA bases.[42] Therefore, outside electrostatic interaction is the most plausible binding mode between C^2–C^4 complexes and duplex DNA.

2.2.2. DNA cleavage activity. In order to evaluate the ability of the new ligands and corresponding Cu(II) complexes to act as metallo-nucleases, DNA cleavage on plasmid ϕX174 phage DNA was monitored by gel electrophoresis. Supercoiled ϕX174 phage DNA was incubated with different concentrations of the compounds, in phosphate buffer (pH 7.2) for 18 h at 37 °C. The naturally occurring supercoiled form (Form I), when nicked, gives rise to an open circular relaxed form (Form II) and upon further cleavage, results in the linear form (Form III). When subjected to gel electrophoresis, relatively fast migration is observed for Form I. Form II migrates slowly and Form III migrates between Forms I and II. The distribution of the three DNA forms in the agarose gel electrophoresis provides a measure of the extent of DNA cleavage. Fig. 7 shows the electrophoretic pattern of plasmid DNA treated with C^1–C^4, where it can be observed that these Cu(II) complexes were able to induce conformational changes in DNA and to promote a concentration-dependent DNA cleavage. Control experiments revealed that no measurable DNA cleavage occurred when ϕX174 phage DNA was incubated with either 250 μM of the non-metallated ligands or $Cu(CF_3SO_3)_2$, clearly indicating that the observed cleavage was due to the metal complexes action.

From the gel electrophoresis analysis (Fig. 7) it is possible to conclude that the cleavage activity is proportional to the concentrations of C^1–C^4. All the complexes could convert the supercoiled DNA (Form I) to nicked DNA (Form II) and even to linear DNA (Form III). From all the complexes, C^2 and C^3 present the highest DNA cleavage activity since the linear DNA was formed even at very low concentration of these complexes (*ca.* 5 μM). In case of C^2, at 5 μM around 55% of the initial supercoiled DNA (Form I) was converted into nicked (53%) and linear DNA form (2%). At 10 μM the cleavage of supercoiled DNA was already *ca.* 90% and, for higher concentrations, no supercoiled form is observed. For C^3, the behavior is quite similar but the cleavage of supercoiled DNA to linear form is not so efficient and a higher percentage of nicked DNA remains, even at high concentrations. In the case of the morpholine complex derivative (C^4), the linear form was almost not observed (2% at $[C^4] =$ 250 μM) indicating lower activity when compared with the other two Cu(II) complexes bearing cyclic amine derivatives.

2.2.3. Mechanistic investigation of the DNA cleavage reaction. In general, metal-mediated DNA cleavage occurs through one of three different pathways, including photocleavage, hydrolysis and oxidative cleavage. To get insight on the mechanism involved in the strong cleavage activity observed, the copper-mediated DNA cleavage was investigated under different experimental conditions (see Fig. 8). Nevertheless, the results obtained without any additive indicate very high "self-activating" nuclease effect.

As most of the copper(II) complexes only accomplish DNA cleavage in the presence of redox agents, two additives were tested, namely ascorbic acid (AA) and H_2O_2 (Fig. 8a and b). AA and H_2O_2 are very important for the action of redox-active "chemical nucleases" that are effective cleavers of DNA, because they are required to initiate and sustain the radical reaction. The effect of adding AA (10 μM, lanes 2, 4 and 10) or H_2O_2 (50 μM, lanes 3, 4 and 11) was evaluated and the result showed that both agents could dramatically enhance the cleavage activity, converting supercoiled DNA to small fragments which could not be easily detected by gel electrophoresis

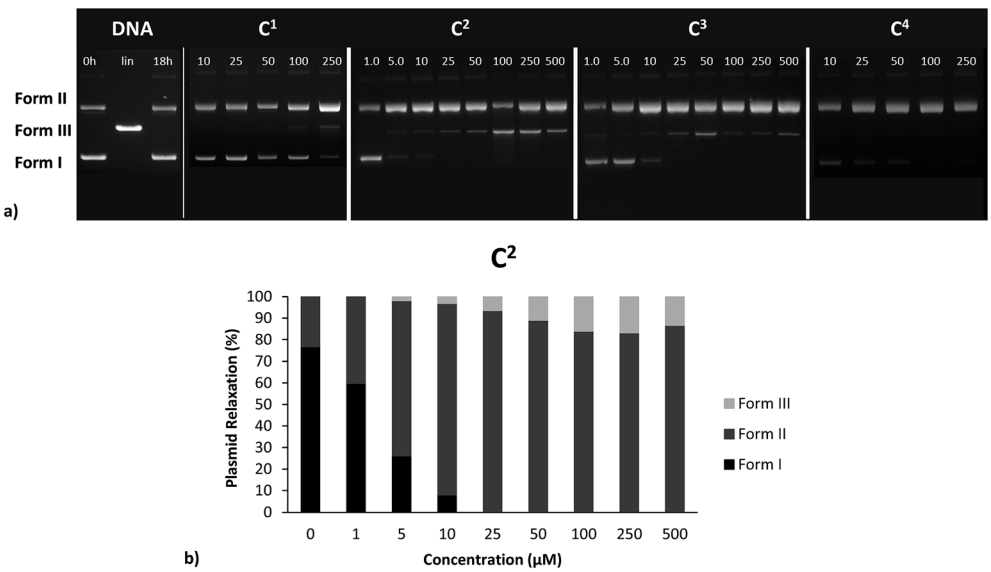

Fig. 7 (a) Agarose gel electrophoresis patterns for the cleavage of supercoiled ϕX174 phage DNA by C^1–C^4 complexes after 18 h of incubation at 37 °C in phosphates buffer (pH 7.2) and (b) percentage of plasmid relaxation for C^2. Forms I, II and III are supercoiled, nicked circular and linear forms of DNA, respectively.

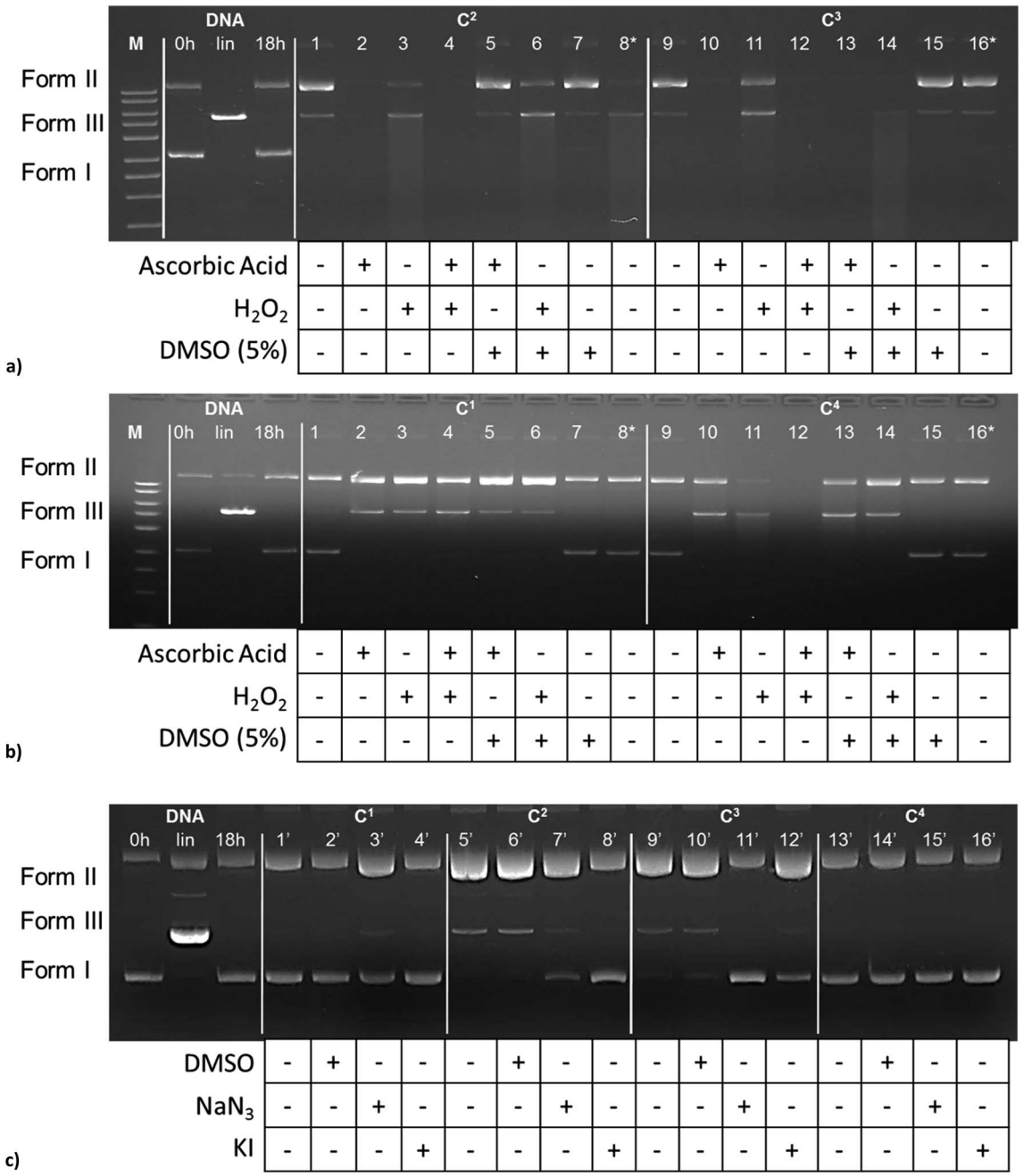

Fig. 8 Cleavage of supercoiled ϕX174 DNA by Cu(II) complexes (a) C^2 and C^3 and (b) C^1 and C^4 in the presence of reducing (ascorbic acid, 10 μM), oxidizing agents (H_2O_2, 50 μM), hydroxyl radical scavenger (DMSO, 5%) or in the dark (*), and (c) C^1–C^4 in the presence of hydroxyl radical scavenger (DMSO, 80 mM) and singlet oxygen species scavengers (NaN_3 and KI, 80 mM), after 18 h of incubation at 37 °C in phosphate buffer (pH 7.2), DNA lin – linear DNA obtained by digestion with XhoI. Forms I, II and III are supercoiled, nicked circular and linear forms of DNA, respectively.

(lanes 2–4 and 10–12). This suggests that the redox process is highly enhanced by the use of reducing/oxidant external agents.

To identify the reactive oxygen intermediates which might be formed in the DNA cleavage process, experiments in the presence of a variety of radical scavengers were also carried out (Fig. 8). DMSO was found to have little effect on the DNA cleavage reaction (lanes 7, 15 and 2′, 6′, 10′, 14′), indicating that hydroxyl radicals are not involved. Additionally, this conclusion was corroborated by fluorescent methods using different dyes, such as terephthalic acid (TPA) and 1,3-diphenyl-isobensofuran (DPBF) (results not shown).

The DNA cleavage could be inhibited when NaN_3 or KI were added to the system (Fig. 8c, lanes 3′–4′, 7′–8′, 12′–13′, 15′–16′), particularly in case of C^2 and C^3. These results suggested the participation of singlet oxygen as active species. Moreover, the dramatic cleavage activity enhancement observed by the addition of H_2O_2 and AA on the reaction catalyzed by C^1–C^4 further supported the oxidative mechanism of action.

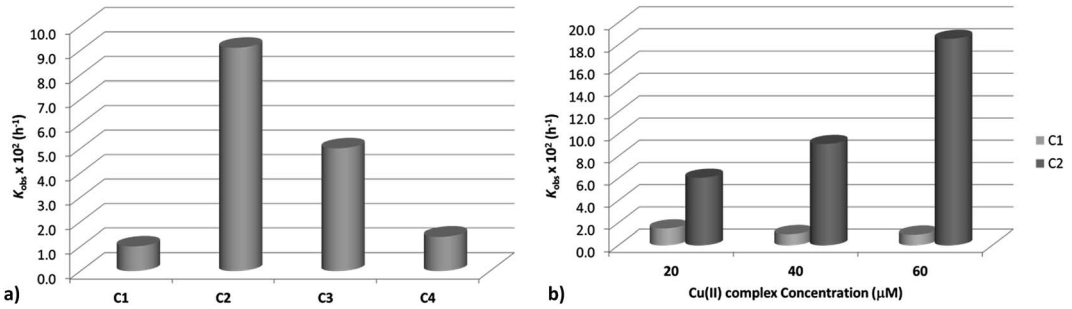

Fig. 9 k_{obs} for the cleavage of supercoiled ϕX174 DNA by Cu(II) complexes (a) C^1–C^4 at 40 μM and (b) C^1 and C^2 at indicated concentration, after incubation over time at 37 °C, in phosphate buffer (pH 7.2).

The photochemical cleavage pathway was excluded by performing control experiments in the absence of light. Comparison of lines 1 and 9 with 8* and 16* respectively, in Fig. 8a and b, confirms that the process is not photochemically activated since the DNA cleavage extend is the same in the presence (1 and 9) or in absence (8* and 16*) of light.

To quantify the nuclease activity of the complexes, the reaction that leads to formation of nicked circular DNA (Form II) from the supercoiled (Sc, Form I) over various concentrations of complexes (20–60 μM) and constant DNA concentration was followed over time (0–22 h). The results of gel electrophoresis were subjected to densitometric quantification and the kinetic parameters were analyzed by assuming a simple pseudo first-order process for conversion of Form I to Form II. The rate constants (k_{obs}) were determined from the plot of ln(% Sc DNA) *versus* time at different concentrations, and in Fig. 9a the k_{obs} obtained for 40 μM of complex are presented. The higher k_{obs} values for C^2 are clearly indicative of the best nuclease activity within this family, which follows the order $C^2 > C^3 > C^4 > C^1$. This effect is even more visible if we represent the k_{obs} *vs.* concentration of complexes (Fig. 9b).

Overall, the DNA cleavage studies of C^2–C^4 complexes showed their remarkable self-activated nuclease activity. For the most active complexes (C^2 and C^3), the activity seems to involve reactive oxygen species as showed by the moderate inhibitory effects caused by the presence of the radical scavengers NaN_3 and KI. Nevertheless, the hydrolytic pathway can not be completely ruled out, as these complexes still showed strong nuclease activity even in the presence of the radical scavengers.

If we consider the cyclic amine ring as a centroid, the distances between the two centroids in the same Cu(II) molecule are about 12.1 Å, twice the distance between adjacent phosphorus atoms of the phosphodiester in the double helix DNA backbone (2 × *ca.* 6 Å).[43] This suggests that the two protonated amines can interact with alternate phosphodiester groups in a DNA strand. This interaction between neighboring phosphoryl oxygen atoms and the protonated amine may lead to more favorable electrostatic interactions, allowing the DNA to be cleaved more readily. Therefore, the higher activity of C^2 and C^3 can be attributed to their structure matching the phosphodiester backbone of the nucleic acids and cooperative interaction from the highly active Bpy–Tpy–Cu(II) moiety and two positive amine groups. This may also explain the lower activity observed for C^4 complex, where the presence of a oxygen atom in the morpholine ring may delocalize the positive charge of the amine and decrease its ability to interact with phosphodiester negatively charged backbone.

2.3. Cell-based studies

The high DNA cleavage ability displayed by the complexes encouraged us to evaluate their cellular uptake and cytotoxicity. The cytotoxic activity of all ligands, Cu(II) complexes and $CuCl_2$ was assayed in the A2780/A2780cisR ovarian cisplatin sensitive/resistant cancer cells by a colorimetric method (MTT assay). Comparison between the activity of the reference drug cisplatin and the activity of these compounds was performed in this cell pair. Dose–response curves after 24 and 72 h exposure were obtained by using an appropriate range of concentrations. IC_{50} values were calculated and are presented in Table 5.

After 72 h of incubation, C^1–C^4 presented high cytotoxic activity, surpassing cisplatin in both cell lines. Moreover, all complexes were able to overcame resistance in the A2780cisR cells when compared to cisplatin. Bipyridine (L^1) and its derivatives (L^2–L^4) displayed lower cytotoxic activity than the corresponding complexes, with IC_{50} values that ranged from 27–94 μM in the A2780 cell line and 44–200 μM in the A2780cisR cell

Table 5 IC_{50} values for A2780 ovarian carcinoma cells and the cisplatin-resistant variant A2780cisR after 24 h and 72 h of continuous treatment with terpyridine, and the mixed Cu(II) complexes (C^1–C^4), $CuCl_2$ and the reference drug cisplatin

	IC_{50} (μM)		
	24 h	72 h	
Compounds	A2780	A2780	A2780cisR
Terpyridine	16.3 ± 5.2	0.93 ± 0.3	4.19 ± 1.3
C^1	20.9 ± 3.4	0.89 ± 0.3	2.05 ± 1.2
C^2	14.6 ± 2.3	0.47 ± 0.2	1.15 ± 0.6
C^3	20.5 ± 5.1	0.27 ± 0.1	0.99 ± 0.6
C^4	17.9 ± 5.0	0.26 ± 0.1	0.88 ± 0.4
$CuCl_2$	—	>100	≫200
Cisplatin	16.9 ± 2.4	1.30 ± 0.5	16.05 ± 1.2

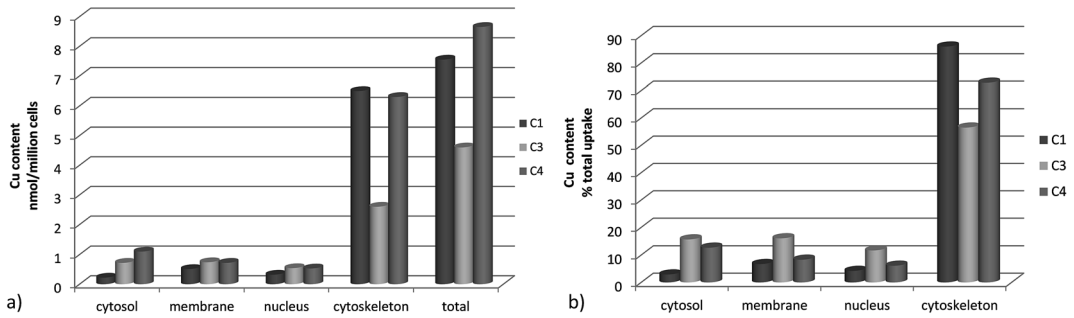

Fig. 10 The subcellular distribution (copper content) of C^1, C^3 and C^4 into the A2780 cells expressed as: (a) nmol of Cu per 10^6 cells; (b) percentage of total copper uptake by the cells. Cells were incubated with the compounds at a concentration equivalent to the IC_{50} values found at 24 h challenge (20 μM). The cytosol, membrane/particulate, nuclear and cytoskeletal fractions were extracted and their copper content determined by ICP-MS.

line. Complexes containing cyclic amine derived bipyridines were much more active (two to three fold) than the parental complex $\mathbf{C^1}$ that contains the non substituted bipyridine.

Cellular uptake studies were performed to evaluate cell permeability in A2780 cells. Furthermore, and to ascertain if the cellular toxicity is related to DNA cleavage, sub-cellular fractioning were also performed. Cells were incubated for 24 h with $\mathbf{C^1}$, $\mathbf{C^3}$ and $\mathbf{C^4}$ at 20 μM, a concentration equivalent to the IC_{50} found for these compounds (Table 5). The amount of copper in the cytosolic, membrane/particulate, nuclear and cytoskeletal fractions of the A2780 cancer cells was quantified by ICP-MS. Results in Fig. 10 show that the three tested complexes ($\mathbf{C^1}$, $\mathbf{C^3}$ and $\mathbf{C^4}$) present similar profiles, *i.e.*, low retention in the cytosol and membranes and a high amount in the cytoskeleton, particularly for $\mathbf{C^1}$ and $\mathbf{C^4}$. Although $\mathbf{C^3}$ shows a lower total uptake, its higher accumulation in the nucleus, membranes and cytosol could probably contribute to confer a high cytotoxic activity.

Given the role of the cytoskeleton in cell transformation and in biological processes such as cell division and cell migration it is pertinent to consider that the cytoskeleton could be a target for these new Cu(II) complexes. In fact the dysfunction of the cytoskeleton is often associated with pathologies such as the onset of metastases, and hence a potential target of interest in numerous therapies.[44]

A small part of complexes (5–10%) is localized in the nuclear fraction, and consequently could damage DNA. Therefore, a comet assay was performed to evaluate DNA damage of A2780 cells after exposure to the different Cu(II) complexes. This assay allows the detection of early nuclear changes in the cells, as well as changes on chromatin organization within a single cell. As seen in Fig. 11, the Cu(II) complexes induced DNA strand breaks in A2780 cells, particularly in the case of $\mathbf{C^1}$, $\mathbf{C^2}$ and $\mathbf{C^4}$. This result further demonstrates the ability of these Cu(II) complexes to induce DNA damage.

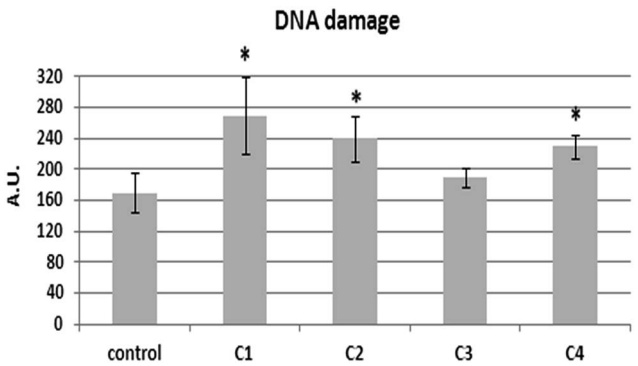

Fig. 11 DNA damage of A7280 cells. Cells were exposed to C^1–C^4 at 20 μM for 24 h; Control: non-exposed cells. Data are presented as average ± standard deviation. (*) stands for statistical significant differences ($p < 0.05$). A.U. stands for arbitrary units.

3 Conclusions

New mixed Bpy–Tpy–Cu(II) complexes were isolated and characterized after reaction of equimolar amounts of Cu(II) with terpyridine and 2,2′-bipyridine derivatives with different cyclic amines. All new complexes show high antitumor activity in ovarian carcinoma A2780 cells, being three to five times more cytotoxic than cisplatin, at 72 h of exposure. Additionally, complexes $\mathbf{C^1}$–$\mathbf{C^4}$ show good activity in the cisplatin-resistant cells A2780cisR, with lower resistance factors than cisplatin. The four complexes tested exhibit similar cellular uptake and distribution profiles with preferential localization in the cytoskeleton.

These new complexes present an impressive plasmid DNA cleaving ability, triggering double-strand DNA breaks in the absence of any exogenous oxidant or reducing agent. After binding to DNA, the complexes cleave the DNA strands by a self-activating mechanism. The cleavage may be carried out *via* an oxidative pathway, but no reductant or oxidant is needed. However, one cannot exclude the possible involvement of hydrolytic reactions catalyzed by the complexes. The enhanced cleavage activity observed for $\mathbf{C^2}$ and $\mathbf{C^3}$ complexes can be attributed to electrostatic interaction between the positive protonated cyclic amines of the complexes and the negative phosphodiester moiety in the DNA backbone. In $\mathbf{C^4}$, delocalization of the positive charge by the presence of the oxygen in the amine ring may lead to a lower electrostatic interaction.

4 Experimental section

4.1. General procedures

All chemicals used were p.a. grade. The chemical reactions were followed by TLC. ^{1}H and ^{13}C NMR spectra were recorded on a Varian Unity 300 MHz spectrometer, and chemical shifts are given in ppm, referenced with the residual solvent resonances relative to $SiMe_4$. IR spectra were recorded in KBr pellets on a Bruker Tensor 27 spectrometer. C, H and N analyses were performed on an EA 110 CE Instruments automatic analyzer. The EPR spectra were recorded at 77 K (on glasses prepared by freezing solutions in liquid nitrogen) with a Bruker ESP 300E X-band spectrometer coupled to a Bruker ER041 X-band frequency meter (9.45 GHz) operating at 100 KHz. The cyclic voltammetry studies were performed under dinitrogen using a potentiostat/galvanostat Radiometer Analytical Voltammetry PST050 VoltaLab® equipment.

4.2. Synthesis of the ligands

4.2.1. Synthesis of 2,2′-bipyridine-4,4′-diol.[21] To a solution of 4,4′-dimethoxy-2,2′-bipyridine (1 g; 4.6 mmol) in acetic acid (60 mL) was added bromhidric acid (16 mL, 92 mmol). The reaction mixture was left under reflux for approximately 72 h and then the solvent was removed under vacuum. The solid residue was dissolved in water and neutralized with ammonium hydroxide. The white precipitate which formed was filtered and dried. Yield 99%. ^{1}H NMR (300 MHz, CD_3OD): δ 8.18 (2H, s, $H_{aromatic}$), 7.24 (2H, s, $H_{aromatic}$), 6.74 (2H, s, $H_{aromatic}$); ESI-MS (MeOH): $(m/z) = 187.0$ $[M - H]^-$.

4.2.2. General procedure for the synthesis of derivatized bipyridine ligands (L^1–L^4). To a solution of 2,2′-bipyridine-4,4′-diol (0.800 g, 4.3 mmol), potassium carbonate (3.526 g, 25.5 mmol) and potassium iodide (catalytic amount) in anhydrous DMF (20 mL) was added 12.8 mmol of the cyclic amine (1-(2-chloroethyl)pyrrolidine, 1-(2-chloroethyl)piperidine or 4-(2-chloroethyl)morpholine). The mixture was stirred at 75 °C for 72 h under N_2. Then the solvent was removed and the residue was purified by column chromatography (100% CH_2Cl_2 to 49/49/2 CH_2Cl_2/MeOH/NH_4OH). The three compounds were obtained as bright-white solids.

4.2.2.1. 4,4′-Bis(2-(pyrrolidin-1-yl)ethoxy)-2,2′-bipyridine (L^2). Yield 51%. ^{1}H NMR (300 MHz, CD_3OD): δ 8.48 (2H, d, CH_{bpy}), 7.89 ppm (2H, s, CH_{bpy}), 7.07 (2H, dd, CH_{bpy}), 4.38 (4H, t, CH_2), 3.18 (4H, t, CH_2), 2.90 (8H, m, CH_2 *ca.*), 1.92 (8H, m, CH_2 *ca.*); ^{13}C RMN (75 MHz, CD_3OD): δ 167.42, 158.72, 151.60, 112.20, 109.00, 67.31, 55.63, 55.42, 24.16. ESI-MS (MeOH): $(m/z) = 383.3$ $[M + H]^+$; CHN (%): experimental 13.9 N, 65.6 C, 8.4 H; calculated for $C_{22}H_{30}N_4O_2 \cdot H_2O$ 14.0 N, 65.9 C, 8.1H.

4.2.2.2. 4,4′-Bis(2-(piperidin-1-yl)ethoxy)-2,2′-bipyridine (L^3). Yield 50%. ^{1}H NMR (300 MHz, $CDCl_3$): δ 8.45 (2H, d, CH_{bpy}), 7.95 ppm (2H, d, CH_{bpy}), 6.85 (2H, dd, CH_{bpy}), 4.31 (4H, t, CH_2), 2.86 (4H, t, CH_2), 2.59 (8H, m, CH_2 *ca.*), 1.66 (8H, m, CH_2 *ca.*), 1.54 (4H, m, CH_2 *ca.*). ^{13}C RMN (75 MHz, $CDCl_3$): δ 165.89, 157.82, 150.12, 111.26, 106.88, 66.07, 57.60, 55.02, 25.94, 24.15. ESI-MS (MeOH): $(m/z) = 411.4$ $[M + H]^+$; CHN (%): experimental 13.0 N, 67.6 C, 9.2 H; calculated for $C_{24}H_{34}N_4O_2 \cdot H_2O$ 13.1 N, 67.3 C, 8.8 H.

4.2.2.3. 4,4′-Bis(2-morpholinoethoxy)-2,2′-bipyridine (L^4). Yield 56%. ^{1}H NMR (300 MHz, $CDCl_3$): δ 8.45 (2H, dd, CH_{bpy}), 7.96 ppm (2H, t, CH_{bpy}), 6.84 (2H, dt, CH_{bpy}), 4.27 (4H, td, CH_2), 3.72 (8H, dd, CH_2 *ca.*), 3.46 (1H, d, CH_2 *ca.*), 2.84 (4H, dt, CH_2), 2.58 (8H, d, CH_2 *ca.*). ^{13}C RMN (75 MHz, $CDCl_3$): δ 165.87, 157.88, 150.29, 111.44, 106.88, 67.00, 65.97, 57.43, 54.18. ESI-MS (MeOH): $(m/z) = 415.3$ $[M + H]^+$; CHN (%): experimental 13.0 N, 61.6 C, 7.9 H; calculated for $C_{22}H_{30}N_4O_4 \cdot H_2O$ 13.0 N, 61.1 C, 7.5 H.

4.3. Synthesis of the copper(II) complexes

4.3.1. General procedure for the synthesis of bipyridine–terpyridine–copper(II) complexes. To a solution of bipyridine ligands L^1–L^4 (0.100 g, 0.24 mmol) and terpyridine (0.056 g, 0.24 mmol) in acetonitrile (6 mL), copper(II) triflate was added (0.24 mmol). The mixture was stirred at room temperature for 2 h. The solution was then concentrated, and diethyl ether and NH_4PF_6 were added to help the complex precipitation. The recovered precipitates were dried under vacuum and formulated as C^1–C^4.

4.3.1.1. Bipyridine–terpyridine–copper(II) complex (C^1). $m = 0.270$ g; 87% yield. CHN (%): experimental 8.62 N, 36.50 C, 3.13 H; calculated for $C_{25}H_{19}CuN_5^{2+} \cdot 2PF_6^- \cdot 4H_2O$ 8.59 N, 36.84 C, 3.34 H. MALDI-TOF-MS (DHB matrix): 452.09 $[M^+]$.

4.3.1.2. 4,4′-Bis(2-(pyrrolidin-1-yl)ethoxy)–2,2′-bipyridine–terpyridine–copper(II) complex (C^2). $m = 0.249$ g; 72% yield; CHN (%): experimental 8.89 N, 36.11 C, 3.93 H; calculated for $C_{37}H_{43}CuN_7O_2^{4+} \cdot 4PF_6^- \cdot 1.5MeCN$ 9.00 N, 36.32 C, 3.62 H. MALDI-TOF-MS (DHB matrix): 678.26 $[M^+]$.

4.3.1.3. 4,4′-Bis(2-(piperidin-1-yl)ethoxy)–2,2′-bipyridine–terpyridine–copper(II) complex (C^3). $m = 0.240$ g; 76% Yield; CHN (%): experimental 7.99 N, 36.75 C, 3.96H; calculated for $C_{39}H_{47}CuN_7O_2^{4+} \cdot 4PF_6^- \cdot 0.5MeCN$ 8.02 N, 36.68 C, 3.73 H. MALDI-TOF-MS (DHB matrix): 706.25 $[M^+]$.

4.3.1.4. 4,4′-Bis(2-morpholinoethoxy)–2,2′-bipyridine–terpyridine–copper(II) complex (C^4). $m = 0.252$ g; 78% yield. CHN (%): experimental 8.69 N, 36.07 C, 3.85H; calculated for $C_{37}H_{43}CuN_7O_4^{4+} \cdot 4PF_6^- \cdot 1.5MeCN$ 8.79 N, 35.46 C, 3.53 H. MALDI-TOF-MS (DHB matrix): 710.25 $[M^+]$.

4.4. X-ray diffraction analysis

Blue crystals of C^3 and C^4 suitable for X-ray diffraction studies were obtained from a acetonitrile solution of the complexes in a saturated chamber of diethyl ether, after standing for some days. The crystals were mounted on a loop with protective oil. X-ray data were collected at 150 K in the ω and φ scans mode on a Bruker APEX II CCD diffractometer using graphite monochromated Mo Kα radiation (0.71073 Å) and operating at 50 kV and 30 mA. Cell parameters were retrieved using Bruker SMART[45] software and refined using Bruker SAINT[45] on all observed reflections. A semi-empirical absorption corrections were applied using SADABS.[46] Structure solution and refinement were performed using direct methods with program SIR97[47] and SHELXL97,[48] both included in the package of

programs WINGX-Version 2013.3.[49] A full-matrix least-squares refinement was used for the non-hydrogen atoms with anisotropic thermal parameters, except for disordered atoms that were refined isotropically. All hydrogen atoms were inserted in idealized positions and allowed to refine riding in the parent carbon atom. Molecular graphics were prepared using ORTEP3.[50] A summary of the crystal data, structure solution and refinement parameters are given in Table 1 ESI.†

4.5. Cyclic voltammetry studies

The redox properties of the complexes and ligands were studied, under nitrogen, by cyclic voltammetry using a potentiostat/galvanostat Radiometer Analytical Voltammetry PST050 VoltaLab® equipment interfaced with a three compartment cell provided with a Pt wire working electrode. $[NBu_4][BF_4]$/0.1 M THF solution was used as electrolyte. The solvent (CH_3CN Sigma-Aldrich) was purified by conventional techniques and distilled immediately before use. The potential values were measured at 200 mV s^{-1} using $[Fe(\eta^5\text{–}C_5H_5)_2]^{0/+}$ as internal reference.

4.6. DNA binding studies

Calf thymus DNA (CT-DNA) sodium salt was purchased from Sigma and was used without further purification. The DNA concentration per nucleotide of stock solutions in phosphate buffer (10 mM, pH 7.2) were determined by absorption spectroscopy at 260 nm, after adequate dilution with the buffer and using the reported molar absorptivity of 6600 M^{-1} cm^{-1}.[51] All measurements involving DNA and the different tested compounds were carried out in phosphate buffer (10 mM, pH 7.2). The absorption and fluorescence titrations were performed by keeping the concentrations of the complex constant, while varying the concentrations of DNA. To obtain the intrinsic binding constant (K_b) all calculations were done considering the DNA concentration in base pairs, and the data were corrected for volume changes.

4.6.1. Absorption spectroscopy studies. UV-Vis absorption spectra were recorded on a Perkin Elmer Lambda 35 spectrometer using 1 cm path-length quartz cells. In order to eliminate any interference of the DNA absorbance in the region of absorbance of the chromophores an equal amount of CT-DNA in phosphate buffer was added to the sample and reference cells. After each addition of CT-DNA, the solution was allowed to equilibrate and the absorption spectrum was recorded until there were no further changes in the absorbance. The K_b was then calculated by fitting the data to a reciprocal plot of $D/\Delta\varepsilon_{ap}$ *versus* D by using the following equation: $D/\Delta\varepsilon_{ap} = D/\Delta\varepsilon + 1/(-\Delta\varepsilon \times K_b)$, in which the concentration of DNA (D) is expressed in terms of base pairs, the apparent molar extinction coefficient $\varepsilon_{ap} = A_{observed}/[complex]$, $\Delta\varepsilon_{ap} = [\varepsilon_a - \varepsilon_f]$ and $\Delta\varepsilon = [\varepsilon_b - \varepsilon_f]$, in which ε_b is the extinction coefficient of the DNA bound complex, and ε_f is the extinction coefficient of the free complex (Scatchard model).[52]

DNA melting experiments were carried out by monitoring the absorption at 260 nm of CT-DNA (100 μM) in the same Perkin-Elmer Lambda 35 spectrophotometer equipped with a Peltier temperature-controlling programmer ETC-717 (±0.1 °C) in phosphate buffer at various temperatures in the presence and absence of the complexes. UV melting profiles were obtained by scanning A260 absorbance monitored at a heating rate of 0.5 °C min^{-1} for solutions of CT-DNA (100 μM) in the absence and presence of different concentrations of copper(II) complexes (10–40 μM) from 30 to 90 °C with the use of the thermal melting program. The melting temperature Tm which is defined as the temperature where half of the total base pairs is unbound was determined from the midpoint of the melting curves.

4.6.2. Fluorescence spectroscopy studies. Fluorescence spectra were recorded in a Perkin Elmer LS 55 fluorescence spectrometer using a quartz cuvette of 1 cm. After each addition of CT-DNA in phosphate buffer, the solution was allowed to equilibrate and the absorption at the excitation wavelength was recorded. The fluorescence spectra were then recorded until there were no further changes in the fluorescence intensity. Complexes $\mathbf{C^1}$–$\mathbf{C^4}$ were excited at 323 nm and the emission spectra were recorded from λ = 335–550 nm, with a scan speed of 300 nm min^{-1}. Emission and excitation slits were chosen in order to maximize the fluorescence intensity.

4.7. DNA cleavage activity

The plasmid DNA used for gel electrophoresis experiments was ϕX174 (Promega). Linear DNA was obtained by digestion with the single-cutter restriction enzyme *Xho*I and used as a reference in agarose gel electrophoresis. DNA cleavage activity was evaluated by monitoring the conversion of supercoiled plasmid DNA (Sc – form I) to nicked circular DNA (Nck – form II) and linear DNA (Lin –form III).

Each reaction mixture was prepared by adding 6 μL of water, 2 μL (200 ng) of supercoiled DNA, 2 μL of 100 mM stock Na_2HPO_4/HCl pH 7.2 buffer solution and 10 μL of the aqueous solution of the complex. The final reaction volume was 20 μL, the final buffer concentration was 10 mM and the final metal concentration varied from 1 to 500 μM. When indicated, the reaction was carried out in the same buffer but in the presence of ascorbic acid (10 μM), H_2O_2 (50 μM), DMSO (5% or 80 mM), NaN_3 (80 mM) and KI (80 mM) or in the dark. Samples were typically incubated for 18 h at 37 °C, except in the case of the kinetics study where times of 1, 2, 4, 6, 8 and 22 h were used. After incubation, 5 μL of DNA loading buffer (0.25% bromophenol blue, 0.25% xylene cyanol, 30% glycerol in water, Applichem) were added to each tube and the sample was loaded onto a 0.8% agarose gel in TBE buffer (89 mM Tris–borate, 1 mM EDTA pH 8.3) containing ethidium bromide (0.5 μg mL^{-1}). Controls of non-incubated and of linearized plasmid were loaded on each gel electrophoresis. The electrophoresis was carried out for 2.5 h at 100 V. Bands were visualised under UV light and images captured using an AlphaImagerEP (Alpha Innotech). Peak areas were measured by denstiometry using AlphaView Software (Alpha Innotech). The photos chosen for this publication were rearranged to show only the relevant samples. All samples in each figure were obtained from the same run. Peak areas were used to calculate the percentage (%) of each form (Sc, Nck and Lin), with a correction factor of 1.47

for the Sc form to account for its lower staining by ethidium bromide.[53] The decrease of Form I over time was fitted as a pseudo-first order kinetics, after logarithmic linearization of the equation $y = (y_0 - a)\exp(-k_{obs}t) + a$, where y_0 is the initial percentage of a form of DNA, y is the percentage of a specific form of DNA at time t, a is the percentage of uncleaved DNA, and k_{obs} is the apparent rate constant.

4.8. Cell viability in human tumoral cell lines

The tumoral cell lines A2780 and A2780cisR were cultured in RPMI 1640 culture medium (Gibco) supplemented with 10% FBS and 1% penicillin/streptomycin at 37 °C in a humidified atmosphere of 95% of air and 5% CO_2 (Heraeus, Germany). The cells were adherent in monolayers and, when confluent, were harvested by digestion with 0.05% trypsin–EDTA (Gibco) and seeded farther apart.

Cell viability was evaluated by using a colorimetric method based on the tetrazolium salt MTT ([3-(4,5-dimethylthiazol-2-yl)-2,5-diphenyltetrazolium bromide]), which is reduced by living cells to yield purple formazan crystals. Cells were seeded in 96-well plates at a density of 1–1.5 $\times$ 10^4 cells per well in 200 μL of culture medium and left to incubate overnight for optimal adherence. After careful removal of the medium, 200 μL of a dilution series of the compounds in fresh medium were added and incubation was performed at 37 °C/5% CO_2 for 24 h and 72 h. The percentage of DMSO in cell culture medium did not exceed 1%. Cisplatin was first solubilized in saline and then added at the same concentrations used for the other compounds. At the end of the incubation period, the compounds were removed and the cells were incubated with 200 μL of MTT solution (500 μg mL^{-1}). After 3–4 h at 37 °C/5% CO_2, the medium was removed and the purple formazan crystals were dissolved in 200 μL of DMSO by shaking. The cell viability was evaluated by measurement of the absorbance at 570 nm using a plate spectrophotometer (Power Wave Xs, Bio-Tek). The cell viability was calculated dividing the absorbance of each well by that of the control wells (cells treated with medium containing 1% DMSO). Each experiment was repeated at least three times and each point was determined in at least six replicates. Statistical analysis was done with GraphPad Prism software.

4.9. Comet assay

The comet assay was performed in A2780 cells to detect the presence of DNA strand breaks. Five different conditions were defined: untreated cells (negative control) and cells treated with **C¹**–**C⁴** at 20 μM. The assay was performed after 24 h exposure, under yellow light, to prevent UV-induced DNA damage and with slight modifications of the protocol described by Nogueira *et al.*[54] Briefly, exposed and non-exposed A2780 cells were adjusted to a concentration of 1 $\times$ 10^4 cells per mL, mixed with 0.5% low melting point agarose, at a ratio of 1 : 10 (v/v) and placed on top of 1% (w/v) normal melting point agarose pre-coated microscope slides. The slides with the embedded cells were immersed into precooled lysing solution (2.5 M NaCl, 100 mM EDTA, 10 mM Tris base and 1% Triton X-100, 10% DMSO, pH 10) at 4 °C for 120 min in the dark. The slides were then placed on a horizontal electrophoresis tray previously filled with freshly prepared cold alkaline buffer and left for 15 min to allow DNA unwinding. Electrophoresis was performed at 43 V, 300 mA for 10 min in alkaline buffer (0.3 M NaOH and 1 mM EDTA, pH 13). Then, slides were neutralized with ice cold 0.4 M Tris–HCl (pH 7.5). Just before analysis cells were stained with 100 μL of ethidium bromide solution (20 μg mL^{-1}).

Cells were counted under inverted fluorescence microscopy. Visual scoring of cellular DNA on each slide was based on the categorization of 100 cells randomly selected. The comet-like formations were visually graded into 5 classes, depending on DNA damage, and scored as described by García *et al.*[55] Positive controls were always included, and consisted of cells previously exposed to 200 μM of H_2O_2, for 1 h. Statistical analyses were performed with GraphPad Prism 6 (GraphPad software, Inc., USA). One-way univariate analysis of variance model (ANOVA) was used. A value of $p < 0.05$ was considered significant.

4.10. Cellular uptake

To explore the uptake of the compounds and its intracellular distribution, A2780 cells (10^6 cells in 5 mL medium) were exposed to **C¹**, **C³** and **C⁴** complexes at 20 μM for 24 h, a concentration equivalent to the IC_{50} values found for a 24 h incubation. After that period, cells were washed with cold PBS and centrifuged to obtain a cellular pellet following a previously described procedure.[56] Cytosol, membrane/particulate, nuclear and cytoskeletal fractions were obtained using a commercial kit (Fraction^{PREP} cell fractionation kit from BioVision) following the manufacturer's recommendations.

The copper content in the different fractions was measured, after digestion, by a Thermo XSERIES quadrupole ICP-MS instrument (Thermo Scientific). Briefly, samples were digested with ultrapure HNO_3, H_2O_2, and HCl in a closed pressurized microwave digestion unit (Mars5, CEM) with medium-pressure HP500 vessels and then diluted in ultrapure water to obtain a 2.0% (v/v) acid solution. The instrument was tuned using a multielement ICP-MS 71 C standard solution (Inorganic Venture). Indium-115 at 10 μg L^{-1} was used as an internal standard.

Acknowledgements

The authors would like to acknowledge FCT for financial support (PTDC/QUI-QUI/114139/2009, PEst-OE/QUI/UI0100/2013, SFRH/BPD/29564/2006 grant to S. Gama, SFRH/BPD/80758/2011 grant to E Palma and FCT Investigator contract to F. Mendes and I. Correia). A. Cruz was funded by the post-doctoral grant (BPD/UI88/2886/2013), from the project "Sustainable Use of Marine Resources" – MARES (CENTRO-07-ST24-FEDER-002033), funded by QREN, Mais Centro – Programa Operacional Regional do Centro e União Europeia/Fundo Europeu de Desenvolvimento Regional. Dr Eugénio Soares from Laboratório Central de Análises, Universidade de Aveiro is acknowledged for the ICP-MS analyses. The IST-UTL Centers of

the Portuguese NMR Network (REM2013, RNNMR) and RECI/QEQ-QIN/0189/2012.

References

1 K. Ghosh, P. Kumar, N. Tyagi, U. P. Singh and N. Goel, *Inorg. Chem. Commun.*, 2011, **14**, 489–492.
2 M. Tian, H. Ihmels and E. Brotz, *Dalton Trans.*, 2010, **39**, 8195–8202.
3 F. Mancin, P. Scrimin and P. Tecilla, *Chem. Commun.*, 2012, **48**, 5545–5559.
4 D. S. Sigman, D. R. Graham, V. D'Aurora and A. M. Stern, *J. Biol. Chem.*, 1979, **254**, 12269–12272.
5 K. Li, L.-H. Zhou, J. Zhang, S.-Y. Chen, Z.-W. Zhang, J.-J. Zhang, H.-H. Lin and X.-Q. Yu, *Eur. J. Med. Chem.*, 2009, **44**, 1768–1772.
6 K. Ghosh, P. Kumar, V. Mohan, U. P. Singh, S. Kasiri and S. S. Mandal, *Inorg. Chem.*, 2012, **51**, 3343–3345.
7 S. Borah, M. S. Melvin, N. Lindquist and R. A. Manderville, *J. Am. Chem. Soc.*, 1998, **120**, 4557–4562.
8 O. Baudoin, M.-P. Teulade-Fichou, J.-P. Vigneron and J.-M. Lehn, *Chem. Commun.*, 1998, **21**, 2349–2350.
9 M. S. Melvin, J. T. Tomlinson, G. R. Saluta, G. L. Kucera, N. Lindquist and R. A. Manderville, *J. Am. Chem. Soc.*, 2000, **122**, 6333–6334.
10 G. Roelfes, M. E. Branum, L. Wang, L. Que and B. L. Feringa, *J. Am. Chem. Soc.*, 2000, **122**, 11517–11518.
11 C. Sissi, F. Mancin, M. Gatos, M. Palumbo, P. Tecilla and U. Tonellato, *Inorg. Chem.*, 2005, **44**, 2310–2317.
12 E. Lamour, S. Routier, J.-L. Bernier, J.-P. Catteau, C. Bailly and H. Vezin, *J. Am. Chem. Soc.*, 1999, **121**, 1862–1869.
13 S. S. Tonde, A. S. Kumbhar, S. B. Padhye and R. J. Butcher, *J. Inorg. Biochem.*, 2006, **100**, 51–57.
14 P. U. Maheswari, S. Roy, H. den Dulk, S. Barends, G. van Wezel, B. Kozlevčar, P. Gamez and J. Reedijk, *J. Am. Chem. Soc.*, 2005, **128**, 710–711.
15 P. U. Maheswari, M. v. d. Ster, S. Smulders, S. Barends, G. P. v. Wezel, C. Massera, S. Roy, H. d. Dulk, P. Gamez and J. Reedijk, *Inorg. Chem.*, 2008, **47**, 3719–3727.
16 A. Kellett, M. O'Connor, M. McCann, M. McNamara, P. Lynch, G. Rosair, V. McKee, B. Creaven, M. Walsh, S. McClean, A. Foltyn, D. O'Shea, O. Howe and M. Devereux, *Dalton Trans.*, 2011, **40**, 1024–1027.
17 L. Li, K. Du, Y. Wang, H. Jia, X. Hou, H. Chao and L. Ji, *Dalton Trans.*, 2013, **42**, 11576–11588.
18 K. Ghosh, P. Kumar, N. Tyagi, U. P. Singh, V. Aggarwal and M. C. Baratto, *Eur. J. Med. Chem.*, 2010, **45**, 3770–3779.
19 C. Santini, M. Pellei, V. Gandin, M. Porchia, F. Tisato and C. Marzano, *Chem. Rev.*, 2013, **114**, 815–862.
20 R. Loganathan, S. Ramakrishnan, E. Suresh, A. Riyasdeen, M. A. Akbarsha and M. Palaniandavar, *Inorg. Chem.*, 2012, **51**, 5512–5532.
21 Y.-R. Hong and C. B. Gorman, *J. Org. Chem.*, 2003, **68**, 9019–9025.
22 H. Hofmeier, E. Herdtweck and U. S. Schubert, *Z. Anorg. Allg. Chem.*, 2004, **630**, 683–688.
23 S.-P. Tang and D.-Z. Kuang, *Acta Crystallogr., Sect. E: Struct. Rep. Online*, 2007, **63**, m3007.
24 V. Uma, M. Kanthimathi, T. Weyhermuller and B. U. Nair, *J. Inorg. Biochem.*, 2005, **99**, 2299–2307.
25 D. Sanna, P. Buglyo, A. I. Tomaz, J. C. Pessoa, S. Borovic, G. Micera and E. Garribba, *Dalton Trans.*, 2012, **41**, 12824–12838.
26 W. E. B. J. Peisach, *Arch. Biochem. Biophys.*, 1974, **165**, 691–708.
27 U. Sakaguchi and A. W. Addison, *Dalton Trans.*, 1979, **4**, 600–608.
28 A. Rockenbauer and L. Korecz, *Appl. Magn. Reson.*, 1996, **10**, 29–43.
29 J. R. Aranzaes, M.-C. Daniel and D. Astruc, *Can. J. Chem.*, 2006, **84**, 288–299.
30 Z.-S. Yang, Y.-L. Wang and G.-C. Zhao, *Anal. Sci.*, 2004, **20**, 1127–1130.
31 G. Tabbì, A. Giuffrida and R. P. Bonomo, *J. Inorg. Biochem.*, 2013, **128**, 137–145.
32 M. Sirajuddin, S. Ali and A. Badshah, *J. Photochem. Photobiol., B*, 2013, **124**, 1–19.
33 J. Liu, T. Zhang, T. Lu, L. Qu, H. Zhou, Q. Zhang and L. Ji, *J. Inorg. Biochem.*, 2002, **91**, 269–276.
34 K. Ashwini Kumar, K. L. Reddy, S. Vidhisha and S. Satyanarayana, *Appl. Organomet. Chem.*, 2009, **23**, 409–420.
35 A. Kumar, J. Prakash Chinta, A. Kumar Ajay, M. Kumar Bhat and C. P. Rao, *Dalton Trans.*, 2011, **40**, 10865–10872.
36 S. Rajalakshmi, T. Weyhermüller, A. J. Freddy, H. R. Vasanthi and B. U. Nair, *Eur. J. Med. Chem.*, 2011, **46**, 608–617.
37 K. Suntharalingam, D. J. Hunt, A. A. Duarte, A. J. P. White, D. J. Mann and R. Vilar, *Chem.–Eur. J.*, 2012, **18**, 15133–15141.
38 W.-Y. Li, J.-G. Xu, X.-Q. Guo, Q.-Z. Zhu and Y.-B. Zhao, *Spectrochim. Acta, Part A*, 1997, **53**, 781–787.
39 J.-H. Li, J.-T. Wang, P. Hu, L.-Y. Zhang, Z.-N. Chen, Z.-W. Mao and L.-N. Ji, *Polyhedron*, 2008, **27**, 1898–1904.
40 W. Saenger, in *Springer Advanced Texts in Chemistry Series*, ed. C. R. Cantor, Springer, New York, 1984, p. 143.
41 X.-L. S. Hao-Yu Shen, H. Xu, J. LI and S.-D. Pan, *Int. J. Electrochem. Sci.*, 2011, **6**, 532–547.
42 R. Pasternack and P. Collings, *Science*, 1995, **269**, 935–939.
43 J. He, P. Hu, Y.-J. Wang, M.-L. Tong, H. Sun, Z.-W. Mao and L.-N. Ji, *Dalton Trans.*, 2008, 3207–3214.
44 I. Nedeva, G. Koripelly, D. Caballero, L. Chièze, B. Guichard, B. Romain, E. Pencreach, J.-M. Lehn, M.-F. Carlier and D. Riveline, *Nat. Commun.*, 2013, **4**, 2165.
45 SMART, SAINT and SADABS, Bruker AXS Inc., Madison, Wisconsin, USA, 2005.
46 S. G. M. Sheldrick, Bruker AXS Inc., Madison, Wisconsin, USA, 2004.
47 A. Altomare, M. C. Burla, M. Camalli, G. L. Cascarano, C. Giacovazzo, A. Guagliardi, A. G. G. Moliterni, G. Polidori and R. Spagna, *J. Appl. Crystallogr.*, 1999, **32**, 115–119.
48 G. M. Sheldrick. Institut fur Anorganische Chemie der Universitat, Tammanstrasse 4, D-3400 Gottingen, Germany, 2008.
49 L. J. Farrugia, *J. Appl. Crystallogr.*, 2012, **45**, 849–854.

50 L. J. Farrugia, *J. Appl. Crystallogr.*, 1997, **30**, 565–566.
51 C. V. Kumar and E. H. Asuncion, *J. Am. Chem. Soc.*, 1993, **115**, 8547–8553.
52 E. H. A. P. C. V. Kumar and W. B. Tan, *Tetrahedron*, 2000, **56**, 7027–7040.
53 N. Butenko, A. I. Tomaz, O. Nouri, E. Escribano, V. Moreno, S. Gama, V. Ribeiro, J. P. Telo, J. C. Pesssoa and I. Cavaco, *J. Inorg. Biochem.*, 2009, **103**, 622–632.
54 P. R. Nogueira, J. Lourenço, S. Mendo and J. M. Rotchell, *Mar. Pollut. Bull.*, 2006, **52**, 1611–1616.
55 O. García, T. Mandina, A. I. Lamadrid, A. Diaz, A. Remigio, Y. Gonzalez, J. Piloto, J. E. Gonzalez and A. Alvarez, *Mutat. Res., Fundam. Mol. Mech. Mutagen.*, 2004, **556**, 25–34.
56 S. Gama, F. Mendes, T. Esteves, F. Marques, A. Matos, J. Rino, J. Coimbra, M. Ravera, E. Gabano, I. Santos and A. Paulo, *ChemBioChem*, 2012, **13**, 2352–2362.